Temperature- and Structural-Parameters-Dependent Characteristics of V-Band Heterojunction FET MMIC DROs

Ken'ichi Hosoya, *Member, IEEE*, Keiichi Ohata, *Member, IEEE*, Takashi Inoue, Masahiro Funabashi, and Masaaki Kuzuhara, *Senior Member, IEEE*

***Abstract*—This paper describes a systematic approach to the design and analysis for dielectric resonator oscillators (DROs). The approach features a temperature- and structural-parameters-dependent dielectric resonator (DR) model and a newly developed temperature-dependent nonlinear FET model. The implementation of these models on a harmonic-balance circuit simulator allows prediction for mechanical tuning characteristics, coupling strength dependencies, and temperature-dependent performance of oscillation frequency, output power, and phase noise of DROs. V-band heterojunction FET monolithic-microwave integrated-circuit DROs utilizing a $\mathrm{TE}_{01\delta}$-mode cylindrical DR were designed and fabricated based on the proposed procedure. Good agreement between the predicted and measured characteristics indicates the validity of our design technique featuring the proposed DR and FET models.**

***Index Terms*—Dielectric resonator oscillators (DROs), dielectric resonators (DRs), FETs, millimeter wave, monolithic microwave integrated circuits (MMICs), oscillators, temperature.**

I. Introduction

DIELECTRIC resonator oscillators (DROs) have been demonstrated at microwave [1]–[6] and millimeter-wave [7]–[9] frequency ranges. They have exhibited excellent phase-noise performance and temperature stability due to the extremely high unloaded quality factor and the small and controllable temperature coefficient of dielectric resonators (DRs) [10], [11].

In the DRO design, it is demanded to simulate dependencies of various characteristics (oscillation frequency f_{osc}, output power P_{out}, and phase noise) on structural parameters of the resonant system such as the distance between the DR top surface and tuning screw and the distance between the DR and microstrip line (MSL). The former parameter (H_2) is often referred to as the air gap by which DRO characteristics can be tuned after assembling. The latter parameter (δ) determines coupling strength between the DR and MSL. Although several authors have reported experimental data on the air-gap tuning characteristics of f_{osc} and P_{out} [1], [2], [4], [6], [19] and the coupling strength dependencies of f_{osc} [6], P_{out} [6], [7], [14], and the phase noise [7], very few theoretical attempts have been made on such characteristics. Rizzoli *et al.* [16] have simulated the air-gap dependence of f_{osc} and P_{out} based on the harmonic-balance method. Seawright *et al.* [14] have predicted P_{out} as a function of δ using a time-domain analysis. However, the method of Rizzoli *et al.* was purely theoretical and was not based on experimental results for the resonant system, which are necessary for realistic DRO design. On the other hand, Seawright *et al.* utilized experimental results for the resonant circuit. Their method, however, was not constructed for systematic studies. Furthermore, the very important parameter of phase noise has not been treated in both attempts. Consequently, a proposal of the systematic design approach, which enables one to predict changes in f_{osc}, P_{out} and phase noise with the structural parameters, is strongly desired.

The specification of frequency stability over a temperature range is another common requirement for many DRO applications. While experimental data on temperature dependencies of f_{osc} and P_{out} for DROs have been extensively reported [1], [2], [4], [6]–[8], [14], [17], [19], little information exists in regard to understanding and estimation of the frequency stability for DROs. Several authors [3], [12], [13] have suggested that temperature sensitivity can be reduced to an acceptable value by choosing a DR with an appropriate temperature coefficient, but they have not provided any quantitative analysis. Tsironis *et al.* [17] have presented an analytical approach to model the temperature dependence of a DRO, giving great insight into the problem. However, their research was inherently based on small-signal analysis and did not provide an accurate prediction of temperature-dependent large-signal behaviors. Abe *et al.* [1], Makino and Hashima [6], and Massias *et al.* [18] have also derived analytical expressions for the temperature stability of DROs, taking into account their large-signal aspects. Their expressions, however, contain the temperature-stability term for an active device [6], [18] or for an unstabilized oscillator [1]. Hence, their method needs a specialized measurement, such as a temperature-dependent load–pull measurement [18], which is generally difficult for most of the DRO designers. To the authors' knowledge, there have been no reports on the nonlinear analysis based on the harmonic-balance or time-domain methods, which enables accurate and direct prediction of temperature dependence of DRO characteristics under large-signal conditions.

Manuscript received October 30, 2001.

K. Hosoya is with the Photonic and Wireless Devices Research Laboratories, NEC Corporation, Tsukuba, Ibaraki 305-8501, Japan (e-mail: k-hosoya@ce.jp.nec.com).

K. Ohata, T. Inoue, and M. Kuzuhara are with the Photonic and Wireless Devices Research Laboratories, NEC Corporation, Otsu, Shiga 520-0833, Japan.

M. Funabashi is with the System ULSI Development Division, NEC Corporation, Nakahara-ku, Kawasaki 221-8666, Japan.

Digital Object Identifier 10.1109/TMTT.2002.807848

The above-mentioned problems can be attributed to the following reasons. A DR coupled to an MSL has usually been modeled as an *RLC* parallel resonant circuit [1], [12], [13], [32] or an *RLC* parallel resonant circuit with an ideal transformer [3], [19]. The values of equivalent circuit elements (R, L, C, and turn ratio k) have been determined as constants, not functions of the structural parameters, nor temperature. This has made it difficult to simulate the dependence of DRO characteristics on structural parameters and temperature.

In [20], the authors derived an equivalent-circuit model for a DR coupled to an MSL, where element parameters depend on the temperature and structural parameters of the resonant system. In this paper, we will implement our DR model on the harmonic-balance circuit simulator, and predict $f_{\rm osc}$, $P_{\rm out}$ and the phase noise of DROs as functions of temperature and structural parameters. A temperature-dependent heterojunction FET (HJFET) nonlinear model is also introduced to predict temperature characteristics of DROs. Based on the proposed method, V-band HJFET monolithic-microwave integrated-circuit (MMIC) DROs are designed, fabricated, and analyzed, utilizing a $\rm TE_{01\delta}$-mode Ba(Mg,Ta)O_3 cylindrical DR. Good agreement between the predicted and measured performance confirms the validity of the proposed design methodology.

II. Structural-Parameters- and Temperature-Dependent DR Model

In this section, we will first review our model for a DR coupled to an MSL [20], where element parameters depend on temperature and structural parameters, as illustrated in Fig. 1.

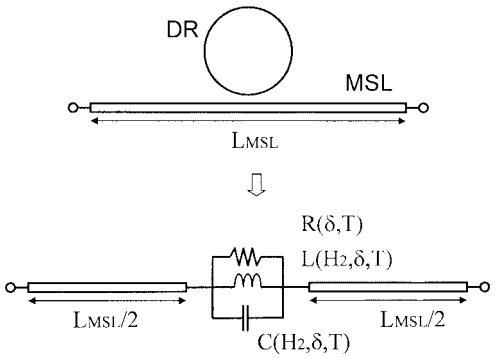

Fig. 1. Equivalent-circuit modeling for DR coupled to an MSL.

Fig. 2 shows the cross-sectional view of the resonant structure. Analysis was performed on a cylindrical resonator of diameter 1.3 mm that is made of Ba(Mg,Ta)O_3 with a relative dielectric constant ε_r of 23.8. The resonator was placed on top of a GaAs substrate mounted on a test fixture with a tuning screw. The air gap H_2 was varied by rotating the tuning screw. The distance δ between the DR and MSL and temperature T were also varied.

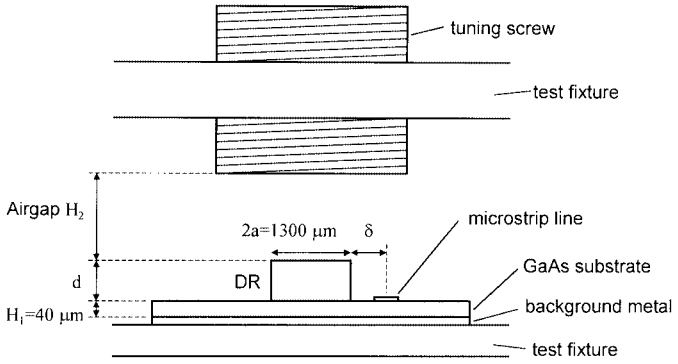

Fig. 2. Cross-sectional view of resonant structure.

The two-port scattering matrix for the resonant structure was measured around the resonant frequency, varying H_2, δ, and T. Values of the resonant angular frequency ω_r, the unloaded Q-factor Q_u, and the coupling coefficient β were extracted from the matrix using the reaction method described by Podcameni *et al.* [21].

The measured ω_r and Q_u as a function of H_2 for the resonator of height 0.55 mm are plotted in Fig. 3(a) and (b). To complement and confirm the measured results, a theoretical calculation was performed for Q_u, taking into account Q factors due to dielectric losses of the resonator and the GaAs substrate and conductor losses of the ground metal and the tuning screw [20]. Each Q factor was calculated using the technique presented by Mongia and Bhartia [22] and Dydyk [23]. The resonant frequency and electromagnetic fields required for the Q-factor calculation were determined by the dielectric waveguide model (DWM) method [24]. A theoretical curve for Q_u is denoted in Fig. 3(b) by a dashed line.

The measured β as a function of δ is denoted in Fig. 3(c) by open dots. The measurement was performed to the range of $\delta \leq 0$ (i.e., the DR is laid on the center conductor of the MSL) to achieve sufficient coupling coefficient in the millimeter-wave frequency range [20]. The coupling coefficient was also verified theoretically using the polarization current method [25]. In the calculation, only a TEM wave was assumed in the MSL and the electrical and magnetic fields in the MSL were calculated by the finite-difference method. Calculated results for β are denoted in Fig. 3(c) by a dashed line.

The temperature characteristics of ω_r, Q_u, and β are also examined in the range from 0 °C to 50 °C, as shown in Fig. 4(a)–(c).

Using the experimental and numerical results described above, ω_r, Q_u, and β were represented as functions of H_2, δ, and T based on the follows assumptions: 1) ω_r and Q_u are independent of δ and 2) β is independent of H_2. These assumptions were consistent with our experimental results. The forms of the functions $\omega_r(H_2, T)$, $Q_u(H_2, T)$, and $\beta(\delta, T)$ were chosen to be consistent with the experimental and theoretical results using appropriate simple analytical functions as follows:

$$\omega_r(H_2, T) = \frac{P_1}{H_2 - P_2} + P_3 + \left(\frac{\Delta\omega_r}{\Delta T}\right)_{H_2=H_{2_0}} (T - T_0) \tag{1}$$

$$Q_u(H_2, T) = P_4 \tanh(P_5 H_2) + P_6 + P_7 H_2 + \left(\frac{\Delta Q_u}{\Delta T}\right)_{H_2=H_{2_0}} \cdot (T - T_0) \tag{2}$$

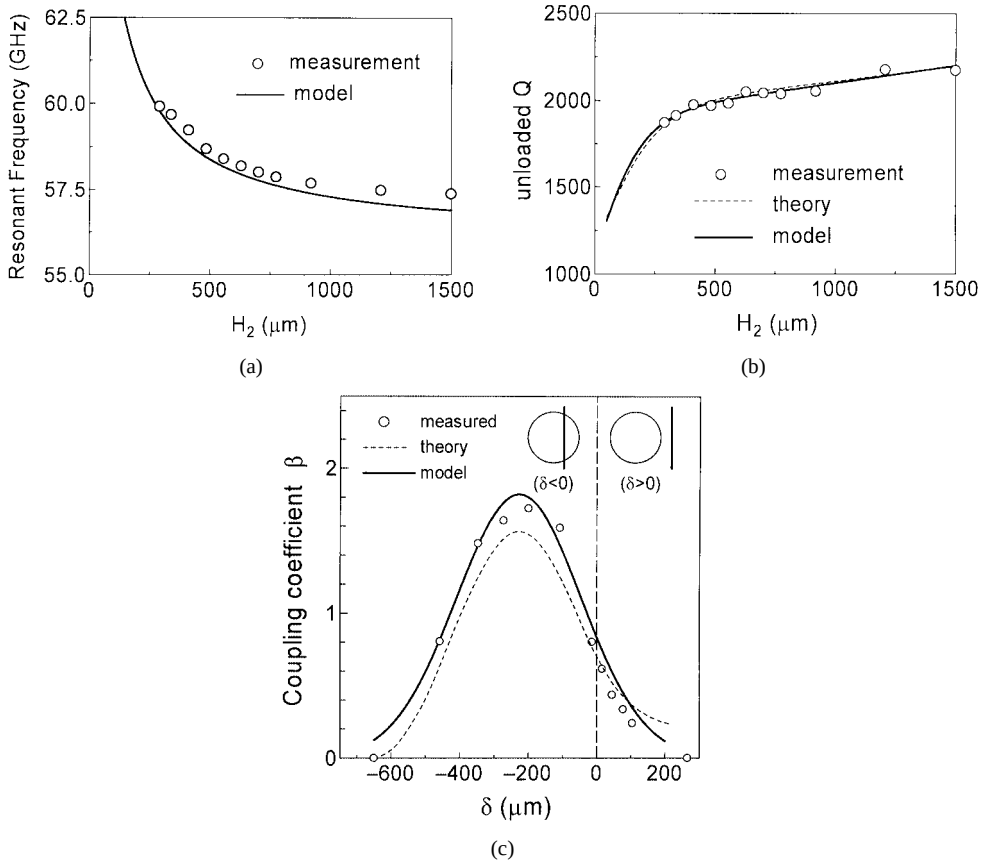

Fig. 3. Comparison between measured, theoretically calculated, and modeled characteristics of resonant structure. (a) Resonant frequency versus air gap. (b) Unloaded Q-factor versus air gap. (c) Coupling coefficient versus distance between resonator and MSL.

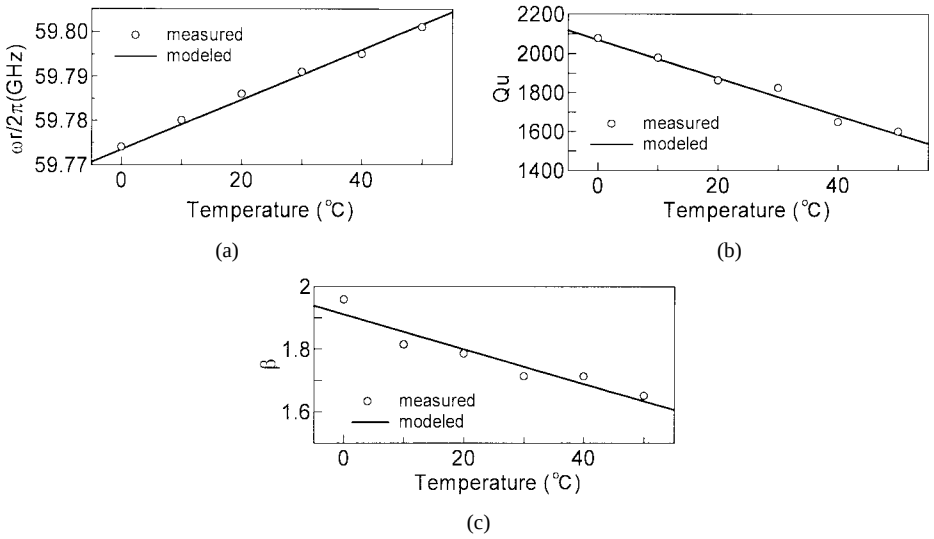

Fig. 4. Temperature characteristics of resonant structure. (a) Resonant frequency. (b) Unloaded Q-factor. (c) Coupling coefficient.

$$\beta(\delta, T) = \left\{ \left(\frac{\Delta\beta}{\Delta T} \right)_{\delta=\delta_0} (T - T_0) + P_8 \right\} \cdot \exp\left\{ -\frac{1}{{P_9}^2} \left(\frac{\delta}{a} - P_{10} \right)^2 \right\}. \quad (3)$$

Meanings of parameters $P_i\,(i = 1\sim10)$ and the determined values for the resonator of height 0.55 mm are described in [20]. In Sections IV and V, we will use various types of DRs with different thickness. Parameters $P_i\,(i = 1\sim10)$ have been extracted for each type of DR. The H_2 dependencies of ω_r and Q_u, the δ dependence of β, and the temperature dependencies of ω_r, Q_u, and β, modeled using (1)∼(3), are shown by solid lines in Figs. 3 and 4. The modeled results were in good agreement with the measurements and theoretical calculations, which validates the adopted functions (1)∼(3).

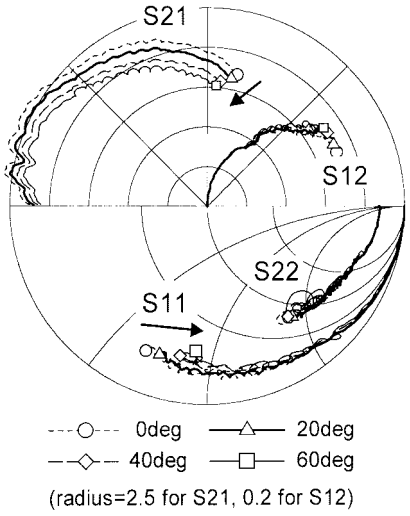

Fig. 5. Measured temperature-dependent S-parameters for HJFET (45 MHz–62.5 GHz).

Using (1)∼(3), the parallel resonant circuit parameters (see Fig. 1) can be written as functions of H_2, δ, and T as follows:

$$R(\delta, T) = 2Z_0\beta(\delta, T) \tag{4}$$

$$L(H_2, \delta, T) = \frac{2Z_0\beta(\delta,T)}{\omega_r(H_2,T)Q_u(H_2,T)} \tag{5}$$

$$C(H_2, \delta, T) = \frac{Q_u(H_2,T)}{2Z_0\omega_r(H_2,T)\beta(\delta,T)} \tag{6}$$

where Z_0 is the characteristic impedance of the MSL to which the DR is coupled. Equations (1)∼(6) are easily implemented into the commercially available microwave computer-aided design (CAD) programs to analyze the DRO performances such as $f_{\rm osc}$, $P_{\rm out}$, and phase noise as functions of temperature and structural parameters.

III. Temperature-Dependent HJFET Large-Signal Model

Temperature characteristics of a transistor, as well as those of a DR, have significant influence on temperature characteristics of DROs. As an active device for V-band MMIC DROs, a 0.15-μm AlGaAs/InGaAs HJFET [26] was employed. Large-signal modeling of the HJFET at room temperature was carried out based on the standard Curtice cubic model [27]. The Curtice cubic model was then modified to represent the temperature dependence of the HJFET characteristics, where several important parameters were expressed as a function of temperature.

The temperature dependence of S-parameters for the HJFET measured in the range from 0 °C to 60 °C is shown in Fig. 5. The dominant features are the decrease in the magnitude of S_{21} and the increase in the phase of S_{11} with increasing temperature. The other S-parameters remain almost unchanged. The drain current at the operated gate bias decreased almost linearly with a slope of -2.8×10^{-2} mA/°C.

The decrease in the magnitude of S_{21} is consistent with the results of Joshin *et al.* [28] for an AlGaAs/InGaAs high electron-mobility transistor (HEMT) and of Angelov *et al.* [29] for an AlGaAs/GaAs HEMT. This is due to the reduction of electron mobility or electron saturated velocity, which results in a reduced transconductance g_m. The increase in the phase of S_{11} has been observed for an AlGaAs/GaAs HEMT [29], although opposite results have been also reported for an AlGaAs/InGaAs HEMT [28]. The main cause for the increase in the phase of S_{11} is the decrease in the gate–source capacitance $C_{\rm gs}$, which has been observed for an InP-based HEMT by Lai *et al.* [30].

To represent these temperature dependencies, three equivalent-circuit parameters $C_{\rm gs0}$, A_0, and A_1 were expressed as linear functions of temperature in a similar manner to Anholt *et al.* [31] and Agarwal and Ho [32] (they expressed transconductance $g_m(T)$ as a linear function of temperature), which were given by

$$C_{\rm gs0}(T) = \frac{\Delta C_{\rm gs0}}{\Delta T}(T - T_0) + C_{\rm gs0}(T_0) \tag{7}$$

$$A_i(T) = \frac{\Delta A_i}{\Delta T}(T - T_0) + A_i(T_0), \qquad i = 0, 1 \tag{8}$$

where $C_{\rm gs0}(T)$ is the gate-to-source capacitance at $V_{\rm GS} = 0$ V and at the ambient temperature T. $A_i(T)$ $(i = 0, 1)$ are coefficients for the cubic equation, where the temperature-dependent drain current $I_{\rm DS}(T)$ is expressed as

$$I_{\rm DS}(T) = \left(A_0(T) + A_1(T)V_1 + A_2V_1^2 + A_3V_1^3\right)\tanh(\gamma V_{\rm out}). \tag{9}$$

V_1 is the input voltage and $V_1 = V_{\rm in} \cdot [1 + \beta_2(V_{\rm out0} - V_{\rm out})]$, where $V_{\rm in}$ is the intrinsic gate-to-source voltage, β_2 is the coefficient for pinchoff change as a function of the intrinsic drain-to-source voltage $V_{\rm out}$, and $V_{\rm out0}$ is the value of $V_{\rm out}$ at which $A_i\,(i = 0\sim3)$ was evaluated. The rates of variation with temperature, $\Delta C_{\rm gs0}/\Delta T$, $\Delta A_i/\Delta T$ $(i = 0, 1)$ were determined to represent the temperature dependencies of the magnitude of S_{21}, the phase of S_{11}, and the drain current $I_{\rm DS}$.

Fig. 6(a) and (b) shows measured and modeled magnitude of S_{21} and phase of S_{11} as a function of temperature. Good agreement between them confirms that (7) and (8) are reasonable expressions to represent temperature characteristics of the HJFET. Note that the temperature-dependent HJFET large-signal model, thus derived, is very simple where only three parameters are considered to be temperature dependent. However, the model is still useful to predict qualitative trends of temperature characteristics of DROs.

IV. Structural-Parameters Dependence of DRO Characteristics

Fig. 7 illustrates the circuit schematic and its equivalent circuit for a MMIC DRO examined here. The DRO consists of a series feedback topology with a 100-μm gatewidth HJFET in a common-source configuration. The resonant circuit, composed of a $\rm TE_{01\delta}$-mode Ba(Mg,Ta)$\rm O_3$ cylindrical DR coupled to an MSL, is connected to the gate terminal of the HJFET. Fig. 8 demonstrates the typical output spectrum for the DRO. A stable oscillation was obtained at around 60 GHz with an output power of 3 dBm. Here, we will attempt to simulate the dependence of the phase noise of DRO on structural parameters utilizing our DR model.

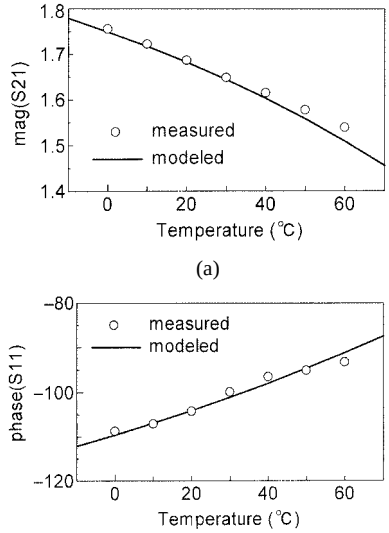

Fig. 6. Comparison between measured and modeled temperature characteristics for an HJFET. (a) Magnitude of S_{21}. (b) Phase of S_{11}.

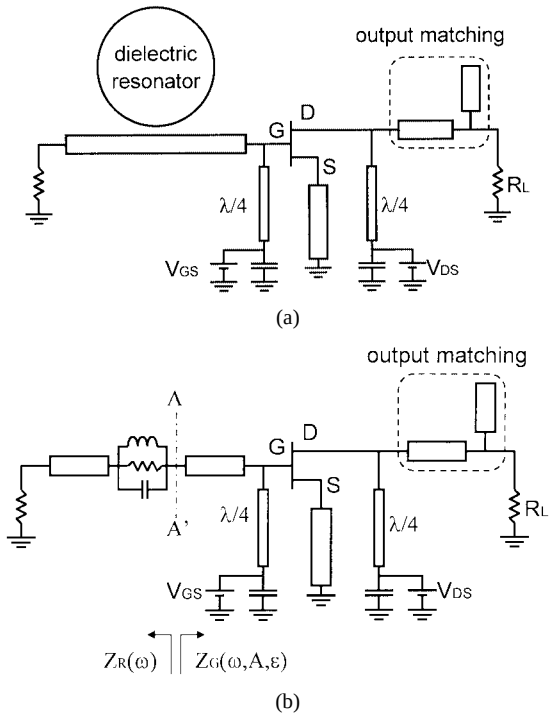

Fig. 7. 60-GHz-band HJFET MMIC DRO. (a) Circuit schematic. (b) Equivalent circuit. DR coupled to MSL in (a) is replaced by *RLC* parallel resonant circuit.

A. Air-Gap Dependence

Measured phase noise at 100-kHz offset as a function of the air gap H_2 is plotted in Fig. 9. The phase noise exhibited a complicated behavior having two minimal values at $H_2 \sim 740$ and $880\,\mu$m. Let us examine this behavior using analytical expressions and the harmonic-balance method together with the present DR model.

The DRO phase noise can be discussed on the basis of a formula for phase noise spectral density $S_\phi(\omega_m)$ of a negative resistance oscillator derived by Kurokawa [33] and later expanded by Riddle and Trew [34]. According to our numerical

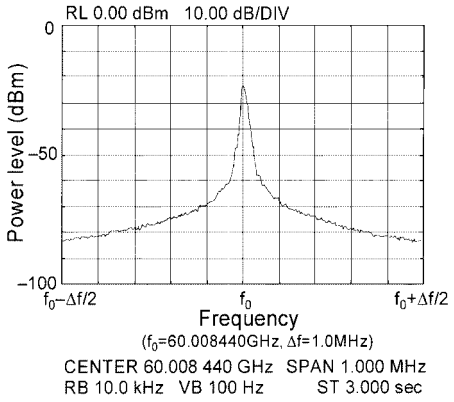

Fig. 8. Typical output spectrum for 60-GHz-band HJFET MMIC DRO. The DRO was assembled in a metal package with a microwave integrated circuit/waveguide transition. The output power of the DRO was divided by a directional coupler between a spectrum analyzer and a power meter for the evaluation of the oscillation spectrum and output-power level, respectively. (The output power of the DRO itself was +3 dBm.)

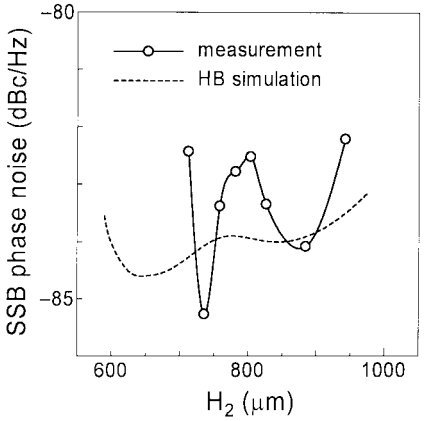

Fig. 9. Air-gap H_2 dependence of SSB phase noise at 100-kHz offset.

calculations, their result can be approximated for DR-stabilized oscillators as follows:

$$S_\phi(\omega_m) = \frac{2n^2(\omega_0)}{A_0^2\omega_m^2} \cdot \frac{1}{\left|\dfrac{dZ_R}{d\omega}\right|_{\omega_0}^2 \sin^2\theta} + \frac{\delta\varepsilon^2(\omega_m)}{\omega_m^2} \cdot \frac{\left|\dfrac{\partial Z_G}{\partial\varepsilon}\right|_{A_0,\omega_0,\varepsilon_0}^2 \sin^2\phi}{\left|\dfrac{dZ_R}{d\omega}\right|_{\omega_0}^2 \sin^2\theta}. \quad (10)$$

Here, $Z_G(A, \omega, \varepsilon)$ is the device impedance and $Z_R(\omega)$ is the resonant circuit impedance, defined in Fig. 7(b). A is the oscillation amplitude. ω_m and ω_0 is the offset angular frequency and oscillation angular frequency, respectively. $n^2(\omega_0)$ denotes the high-frequency white noise and $\delta\varepsilon^2(\omega_m)$ is the low-frequency noise of the active device, which usually has a slope of ω_m^{-1}. ε represents the modulation source. θ is the intersection angle between vectors $\partial Z_G/\partial A$ and $dZ_R/d\omega$ and ϕ is the intersection angle between vectors $\partial Z_G/\partial\varepsilon$ and $\partial Z_G/\partial A$ at operation point $(A_0, \omega_0, \varepsilon_0)$. Note that single sideband (SSB) phase noise is given by $\mathcal{L}(\omega_m) = S_\phi(\omega_m)/2$. According to our experiments, $\mathcal{L}(\omega_m)$ at 100-kHz offset had a slope of ω_m^{-3}, indicating that a

dominant component of the phase noise at 100-kHz offset is the flicker FM noise [36] represented by the second term of (10). We, therefore, consider the second term of (10) in more detail.

The resonant circuit impedance $Z_R(\omega)$ can be expressed in terms of Q_u and β as

$$Z_R(\omega) = Z_0 + \frac{2Z_0\beta(\delta)}{1+jQ_u(H_2)\left(\dfrac{\omega}{\omega_r(H_2)} - \dfrac{\omega_r(H_2)}{\omega}\right)}. \quad (11)$$

Differentiating (11) with respect to ω at resonant frequency ω_r yields

$$\left|\frac{dZ_R}{d\omega}\right|_{\omega_r} = \frac{4Z_0Q_u(H_2)\beta(\delta)}{\omega_r(H_2)}. \quad (12)$$

As shown in Fig. 3(a) and (b), in the range of 600 μm $\leq H_2 \leq$ 1000 μm, ω_r decreases and Q_u increases with increasing H_2, leading to a moderate increase in the frequency sensitivity $|dZ_R/d\omega|_{\omega_r}$. Therefore, referring to (10) and supposing $\omega_r = \omega_0$, a gradual improvement in the phase noise is expected with increasing H_2 if only the changes in $Z_R(\omega)$ are considered. However, as a practical matter, the phase noise at 100-kHz offset represented by the second term of (10) depends on many other factors that are concerned with nonlinear behavior of the circuit. All of four parameters in the term, i.e., $|dZ_R/d\omega|$, $|\partial Z_G/\partial\varepsilon|$, θ, and ϕ vary with H_2 in a complicated manner to satisfy the oscillation condition. As a result, the phase noise as a function of H_2 exhibited two minimal values at $H_2 \sim 740$ and 880 μm. Harmonic-balance simulation utilizing the structural-parameter-dependent DR model seems to explain well the behavior of phase noise as a function of H_2.

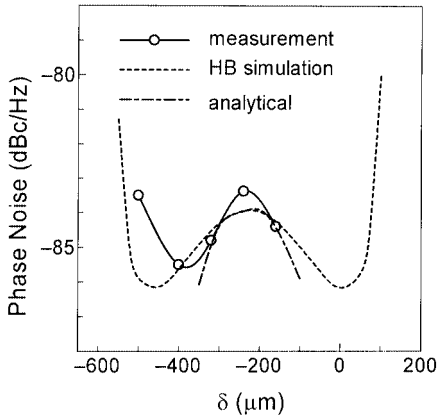

Fig. 10. SSB phase noise at 100-kHz offset as functions of distance between DR and MSL (δ).

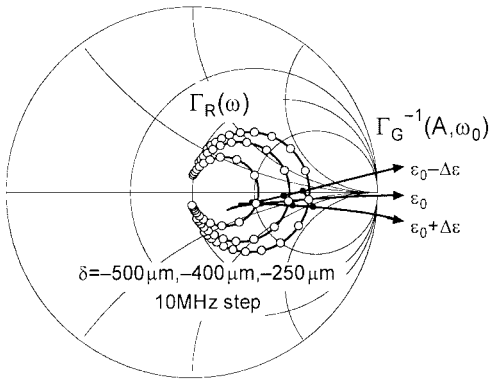

Fig. 11. Calculated reflection coefficients of resonant circuit $\Gamma_R(\omega)$ for $\delta = -200, -400$, and -500 μm. Inversed reflection coefficients of active circuit $\Gamma_G^{-1}(A, \omega_0)$ as functions of oscillation amplitude A for modulation source perturbation $\pm\Delta\varepsilon$ are also displayed.

B. Coupling-Strength Dependence

The phase noise with offset frequency of 100 kHz was also measured varying δ, as plotted in Fig. 10 by open dots. The phase noise exhibited a maximal value around $\delta \sim -250$ μm, where the coupling coefficient β has a maximum value, as demonstrated in Fig. 3(c). Several authors have stated that β has to be small to reduce the phase noise of DROs [4], [5], [9], [13]. However, there has been no established analysis to explain the relation between δ (and, consequently, β) and the phase noise of DROs.

Firstly, we must explain the relationship between Q_u and δ. On the dependence of Q_u on δ, three different results have been reported. Podcameni and Bermudez [15] pointed out that Q_u is degenerated due to the conductor loss of the strip metal when a DR comes up to an MSL. Sanchez *et al.* [37] denoted that it is difficult to asses whether or not Q_u will change by varying δ since both the electromagnetic-field distribution and the conductor loss of the strip metal may be affected. Khanna [38] and Kajfez and Guo [39], on the other hand, showed that δ has little effect on Q_u when shielding conditions are properly chosen. Our experimental results were found to be in good correspondence with the last one (as mentioned in Section II).

It is thus found from (12) that $|dZ_R/d\omega|_{\omega_r=\omega_0}$ is maximized when δ is chosen to give the maximum β. It means that the phase noise is expected to be minimized at $\delta \sim -250$ μm, where β has a maximum value, if only the resonant circuit effects are taken into account. On the contrary, measured phase noise has a maximal value around $\delta \sim -250$ μm, as mentioned above. A harmonic-balance simulation result, indicated in the same figure by a dashed line, is well consistent with the measured result. These results can be explained by analyzing four parameters in the second term of (10).

In Fig. 11, simulated reflection coefficients of the resonant circuit $\Gamma_R(\omega)$ as a function of the angular frequency ω and the inversed reflection coefficients of the active circuit $\Gamma_G^{-1}(A, \omega_0)$ as a function of oscillation amplitude A are displayed on a Smith chart. $\Gamma_R(\omega)$ are plotted for $\delta = -200$, -400 and -500 μm. $\Gamma_G(A, \omega_0)$ are plotted for a modulation source perturbation $\pm\Delta\varepsilon$. The modulation source ε is usually a gate–source voltage V_{gs} for FET-type devices [35] and, thus, we set as $\Delta\varepsilon = \Delta V_{gs} = 0.1$ V. As can be seen from this figure, when δ changes from -250 to -500 μm, the radius of resonant circle becomes small, i.e., $|dZ_R/d\omega|_{\omega_r=\omega_0}$ decreases according to (12). On the other hand, we can see graphically that the sensitivity of the active circuit impedance with respect to the modulation source $|\partial Z_G/\partial\varepsilon|_{A_0,\omega_0,\varepsilon_0}$ is reduced with decreasing δ due to the shift of operation point toward the center of the Smith chart, while angles θ and ϕ remain almost unchanged. Here, the operation point (A_0, ω_0) is given by the intersections of two locus $\Gamma_R(\omega)$ and $\Gamma_G^{-1}(A, \omega_0)$ [33].

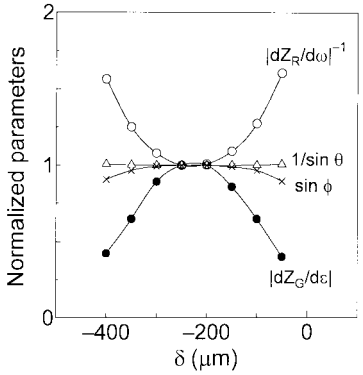

Fig. 12. δ dependencies of parameters in (10) (normalized to values at $\delta = -250$ μm).

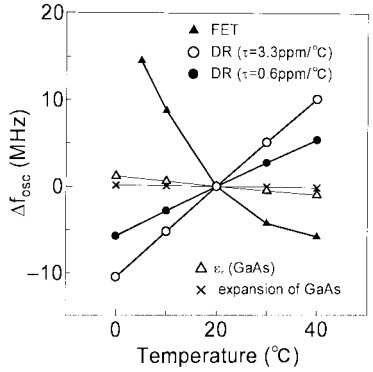

Fig. 13. Calculated oscillation frequency variations due to temperature characteristics of the HJFET, DR coupled to an MSL, dielectric constant of GaAs, and thermal expansion of GaAs substrate. As for the DR coupled to an MSL, results are shown for two types of DRs with the temperature coefficient itself $\tau_{\rm DR}$ of $+0.6$ ppm/°C and $+3.3$ ppm/°C.

Fig. 12 demonstrates these changes of parameters with respect to δ. In this figure, the four parameters $|dZ_R/d\omega|^{-1}$, $|\partial Z_G/\partial\varepsilon|$, $1/\sin\theta$, and $\sin\phi$ are normalized to each value at $\delta = -250$ μm. A product of these four parameters decides the flicker FM noise according to the second term of (10). As is evident from these curves, the maximal value of phase noise at $\delta \sim -250$ μm is attributed to the δ dependence of $|\partial Z_G/\partial\varepsilon|$, which overcomes that of $|dZ_R/d\omega|^{-1}$ around $\delta = -250$ μm. To confirm the above discussion, the deviation of flicker FM noise from the value for $\delta \sim -250$ μm was calculated by substituting computed values of the four parameters into the second term of (10). The resulting curve depicted in Fig. 10 by a dotted–dashed line certainly has a maximal value at $\delta \sim -250$ μm.

To the authors' knowledge, the results demonstrated in this section are the first report on the prevision for dependencies of the DROs' phase noise on the structural parameters. The prevision has been realized by employing the proposed DR model along with the harmonic-balance method. Structural parameters dependence of $f_{\rm osc}$ and $P_{\rm out}$ can be also predicted by our method, although it was not treated in this paper.

V. Temperature Characteristics of DRO

In this section, we will attempt to predict the temperature dependence of $f_{\rm osc}$ and $P_{\rm out}$ based on the harmonic-balance method utilizing the temperature-dependent DR and FET models described in Sections II and III. A 55-GHz-band HJFET MMIC DRO [8] was examined. The circuit configuration is basically the same as that for the 60-GHz-band DRO shown in Fig. 7(a), except that the MSL to which the DR is coupled is terminated by a combination of a resistor and a quarter-wavelength open stub [8].

A. Simulation

In addition to the changes in the DR and HJFET parameters described in Sections II and III, there are several factors responsible for the dependence of DRO performances on temperature, such as the expansion of the GaAs substrate and the variation of the dielectric constant of GaAs, $\varepsilon_{r,\,\rm GaAs}$. The expansion of the GaAs substrate changes the length and width of transmission lines. To determine to what extent each component of a DRO will contribute to the overall temperature sensitivity, the oscillation frequency variation resulting from the change with temperature in HJFET parameters, DR parameters, $\varepsilon_{r,\,\rm GaAs}$, and the expansion of the GaAs substrate are simulated separately by the harmonic-balance method. The results are plotted in Fig. 13. Simulation was carried out for two types of a DR with a temperature coefficient $\tau_{\rm DR}$ of $+0.6$ ppm/°C and $+3.3$ ppm/°C. In the calculation, the thermal expansion coefficient for GaAs of $\alpha_{\rm th} = 6.03 \times 10^{-6}\,({\rm K}^{-1})$ reported by Brice [40] was employed. The temperature dependence of the static dielectric constant for GaAs was expressed according to [41] as $\varepsilon_{r,\,\rm GaAs}(T) = \varepsilon_{r,\,\rm GaAs}(0)(1 + 1.0 \times 10^{-4}T)$, where $\varepsilon_{r,\,\rm GaAs}(0)$ is the dielectric constant at $T = 0$ K. The temperature coefficient of the oscillation frequency due to the variation of DR parameters had the positive sign, whereas that due to the change in FET parameters, the dielectric-constant change and the expansion of the GaAs substrate, had the negative sign. The oscillation frequency drifts caused by the dielectric-constant change and the expansion of the GaAs substrate were found to be insignificant, as compared to those due to the variation of FET and DR parameters. Fig. 14 plots the results of harmonic-balance simulation considering all four origins of temperature variation of the DRO. These results demonstrate that temperature compensation for the $f_{\rm osc}$ may be well achieved by using the DR with $\tau_{\rm DR} = +3.3$ ppm/°C, whereas that for $P_{\rm out}$ is effective for both DROs.

B. Measured Results

Fig. 15 shows the measured temperature characteristics for the DRO using a DR with $\tau_{\rm DR}$ of $+0.6$ ppm/°C and $+3.3$ ppm/°C. Better temperature compensation was accomplished when adopting the DR with $\tau_{\rm DR} = +3.3$ ppm/°C. This result is consistent with the simulation, although temperature coefficients of $f_{\rm osc}$ are somewhat different from the simulated values. The oscillation frequency stability obtained for the DR with $\tau_{\rm DR} = +3.3$ ppm/°C was -1.9 ppm/°C, whereas that for the DR with $\tau_{\rm DR} = +0.6$ ppm/°C was -3.9 ppm/°C. On the other hand, oscillation power variation was almost the same for two types of DRs, which is also consistent with the simulated results. Output power deviation was less than ± 0.8 dB in the temperature range from 0 °C to 40 °C.

To our knowledge, the results described in this section is the first attempt to predict the temperature stability of DROs based

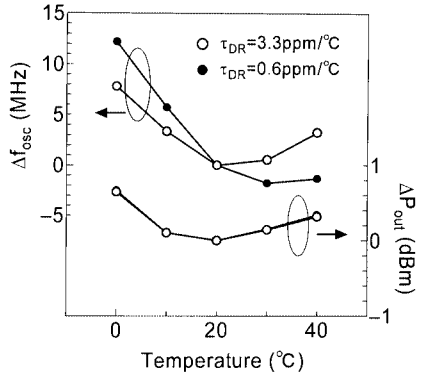

Fig. 14. Simulated temperature characteristics of oscillation frequency and output power for two types of DRs with $\tau_{\rm DR}$ of $+0.6$ ppm/ °C and $+3.3$ ppm/°C. $\Delta f_{\rm osc}$ and $\Delta P_{\rm out}$ represent deviations from these values at 20 °C.

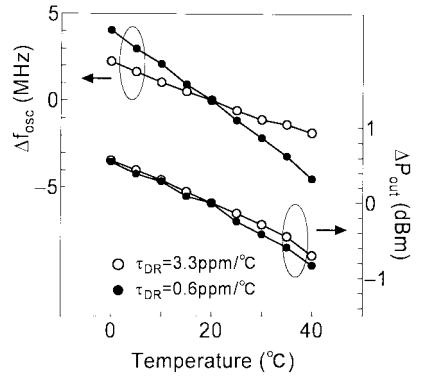

Fig. 15. Measured temperature characteristics for the DRO using two types of DRs with $\tau_{\rm DR}$ of $+0.6$ ppm/°C and $+3.3$ ppm/°C.

on numerical large-signal circuit analysis such as the harmonic-balance or time-domain methods.

VI. Conclusion

A systematic approach to the design and analysis of DROs has been presented. The approach features the equivalent-circuit model for a DR coupled to an MSL, where circuit parameters are dependent on temperature and structural parameters. Implementing this model along with the temperature-dependent HJFET model on a harmonic-balance simulator enabled predictions of DRO characteristics such as oscillation frequency, output power, and phase noise as a function of the temperature and structural parameters. Dependencies of phase noise on structural parameters, and the temperature stability of oscillation frequency and output power were analyzed for V-band MMIC DROs. The analysis was in good agreement with the measurements. These results confirm the validity of the presented design and analysis methodology featuring the temperature- and structural-parameters-dependent DR model.

Acknowledgment

The authors are grateful to Dr. H. Abe, NEC Corporation, Kanagawa, Japan, Dr. M. Ogawa, NEC Corporation, Ibaraki, Japan, Dr. T. Uji, NEC Corporation, Shiga, Japan, Dr. T. Mizuta, NEC Corporation, Shiga, Japan, and Dr. H. Hida, NEC Corporation, Ibaraki, Japan, for their constant encouragement and support through this study.

References

[1] H. Abe, Y. Takayama, A. Higashisaka, and H. Takamizawa, "A highly stabilized low-noise GaAs FET integrated oscillator with a dielectric resonator in the C-band," *IEEE Trans. Microwave Theory Tech.*, vol. MTT-26, pp. 156–162, Mar. 1978.

[2] O. Ishihara, T. Mori, H. Sawano, and M. Nakatani, "A highly stabilized GaAs FET oscillator using a dielectric resonator feedback circuit in 9–14 GHz," *IEEE Trans. Microwave Theory Tech.*, vol. MTT-28, pp. 817–824, Aug. 1980.

[3] K. Kamozaki, "4 GHz miniaturized low noise dielectric resonator stabilized oscillator," in *IEEE MTT-S Int. Microwave Symp. Dig.*, Albuquerque, NM, June 1992, pp. 1305–1308.

[4] K. K. Agarwal, "Dielectric resonator oscillators using GaAs/(Ga,Al)As heterojunction bipolar transistors," in *IEEE MTT-S Int. Microwave Symp. Dig.*, Baltimore, MD, June 1986, pp. 95–98.

[5] K. Ogawa, H. Ikeda, T. Ishizaki, K. Hashimoto, and Y. Ota, "25 GHz dielectric resonator oscillator using an AlGaAs/GaAs HBT," *Electron. Lett.*, vol. 26, no. 18, pp. 1514–1516, Aug. 1990.

[6] T. Makino and A. Hashima, "A highly stabilized MIC Gunn oscillator using a dielectric resonator," *IEEE Trans. Microwave Theory Tech.*, vol. MTT-27, pp. 633–638, July 1979.

[7] G. S. Dow, D. Sensiper, and J. M. Schellenberg, "Highly stable 35 GHz FET oscillator," in *IEEE MTT-S Int. Microwave Symp. Dig.*, Baltimore, MD, June 1986, pp. 589–591.

[8] M. Funabashi, K. Ohata, K. Onda, K. Hosoya, T. Inoue, M. Kuzuhara, K. Kanekawa, and Y. Kobayashi, "A V-band AlGaAs/InGaAs heterojunction FET MMIC dielectric resonator oscillator," in *IEEE GaAs IC Symp. Dig.*, Philadelphia, PA, Oct. 1994, pp. 30–33.

[9] S. Chen, S. Tadayon, T. Ho, K. Pande, P. Rice, J. Adair, and M. Ghahremani, "U-band MMIC HBT DRO," *IEEE Microwave Guided Wave Lett.*, vol. 4, pp. 50–52, Feb. 1994.

[10] J. K. Plourde and C.-L. Ren, "Application of dielectric resonator in microwave components," *IEEE Trans. Microwave Theory Tech.*, vol. MTT-29, pp. 754–770, Aug. 1981.

[11] D. Kajfez and P. Guillon, *Dielectric Resonators*. Norwood, MA: Artech House, 1986.

[12] P. G. Wilson and R. D. Carver, "An easy-to-use FET DRO design procedure suited to most CAD programs," in *IEEE MTT-S Int. Microwave Symp. Dig.*, Long Beach, CA, 1989, pp. 1033–1036.

[13] B. S. Virdee, A. J. Parsons, and R. G. Meadows, "Commercial computer-aided design software optimizes DRO circuit design," in *SBMO Int. Microwave Conf.*, 1993, pp. 457–462.

[14] S. W. J. Seawright, E. B. L. Choo, J. A. C. Stewart, V. F. Fusco, and B. Barnes, "Optimum DRO synthesis," in *Proc. 19th Eur. Microwave Conf.*, London, U.K., 1989, pp. 406–411.

[15] A. Podcameni and L. A. Bermudez, "Large signal design of GaAs FET oscillators using input dielectric resonators," *IEEE Trans. Microwave Theory Tech.*, vol. MTT-31, pp. 358–361, Apr. 1983.

[16] V. Rizzoli, A. Costanzo, and A. Neri, "Analysis and optimization of DRO's using a general-purpose CAD program," *Alta Freq.*, vol. LVII, no. 7, pp. 389–398, Sept. 1988.

[17] C. Tsironis and V. Pauker, "Temperature stabilization of GaAs MESFET oscillators using dielectric resonators," *IEEE Trans. Microwave Theory Tech.*, vol. MTT-31, pp. 312–314, Mar. 1983.

[18] M. Massias, M. J. Hows, and V. Postoyalko, "A novel analysis and design technique for temperature stable DROs," in *Proc. 19th Eur. Microwave Conf.*, London, U.K., 1989, pp. 418–423.

[19] S.-W. Chen, L.-C. Chang, and J. Y. Chin, "An unified design of dielectric resonator oscillators for telecommunication systems," in *IEEE MTT-S Int. Microwave Symp. Dig.*, Baltimore, MD, June 1986, pp. 593–596.

[20] K. Hosoya, T. Inoue, M. Funabashi, and K. Ohata, "Systematic evaluation and analysis for 60-GHz dielectric resonators coupled to a microstrip line on a GaAs substrate," *IEEE Trans. Microwave Theory Tech.*, vol. 46, pp. 352–358, Apr. 1998.

[21] A. Podcameni, L. F. M. Conrado, and M. M. Mosso, "Unloaded quality factor measurement for MIC dielectric resonator applications," *Electron. Lett.*, vol. 17, no. 18, pp. 656–658, Sept. 1981.

[22] R. K. Mongia and P. Bhartia, "Accurate conductor Q-factor of dielectric resonator placed in an MIC environment," *IEEE Trans. Microwave Theory Tech.*, vol. 41, pp. 445–449, Mar. 1993.

[23] M. Dydyk, "Dielectric resonators add Q to MIC filters," *Microwaves*, pp. 150–160, Dec. 1977.

[24] T. Itoh and R. S. Rudokas, "New method for computing the resonant frequencies of dielectric resonators," *IEEE Trans. Microwave Theory Tech.*, vol. MTT-25, pp. 52–54, Jan. 1977.
[25] P. Skalicky, "Coupling coefficient between dielectric resonator and microstrip line," *Electron. Lett.*, vol. 17, no. 2, pp. 99–100, Jan. 1981.
[26] M. Funabashi, K. Hosoya, K. Ohata, K. Onda, N. Iwata, and M. Kuzuhara, "High gain V-band heterojunction FET MMIC power amplifiers," in *IEEE GaAs IC Symp. Dig.*, San Jose, CA, Oct. 1993, pp. 379–382.
[27] W. R. Curtice and M. Ettenberg, "A nonlinear GaAs FET model for use in the design of output circuits for power amplifiers," *IEEE Trans. Microwave Theory Tech.*, vol. MTT-33, pp. 1383–1394, Dec. 1985.
[28] K. Joshin, Y. Mimino, S. Ohmura, and Y. Hirachi, "Noise performance at cryogenic temperatures of AlGaAs/InGaAs HEMT's with 0.15-μm T-shaped WSi_x gates," *IEEE Trans. Electron Devices*, vol. 39, pp. 515–519, Mar. 1992.
[29] I. M. Angelov, I. K. Stoev, Z. G. Ivanov, B. N. Todorov, A. Y. Spasov, E. L. Kollberg, C. O. Lindström, and B. L. Wendemo, "Low noise cooled microwave amplifiers—Simulation and design," *IEEE Trans. Electron Devices*, vol. 40, pp. 389–399, Feb. 1992.
[30] R. Lai, P. K. Bhattacharya, D. Yang, T. L. Brock, S. A. Alterovitz, and A. N. Downey, "Characteristics of 0.8- and 0.2-μm gate length $In_xGa_{1-x}As/In_{0.52}Al_{0.48}As/InP$ $(0.53 \leq x \leq 0.70)$ modulation-doped field-effect transistors at cryogenic temperatures," *IEEE Trans. Electron Devices*, vol. 39, pp. 2206–2213, Oct. 1992.
[31] R. E. Anholt and S. E. Swirhun, "Experimental investigation of the temperature dependence of GaAs FET equivalent circuits," *IEEE Trans. Electron Devices*, vol. 39, pp. 2029–2036, Sept. 1992.
[32] K. K. Agarwal and C. Ho, "Analysis of long-term frequency drift in FET oscillators," *IEEE Trans. Microwave Theory Tech.*, vol. MTT-35, pp. 1328–1333, Dec. 1987.
[33] K. Kurokawa, "Some basic characteristics of broadband negative resistance oscillator circuits," *Bell Syst. Tech. J.*, vol. 48, no. 6, pp. 1937–1955, July 1969.
[34] A. N. Riddle and R. J. Trew, "A new approach to low phase noise oscillator design," in *Proc. IEEE/Cornell Advanced Concepts in High-Speed Semiconductor Devices and Circuits Conf.*, July 1985, pp. 302–311.
[35] H. Rohdin, C.-Y. Su, and C. Stolte, "A study of the relation between device low-frequency noise and oscillator phase noise for GaAs MESFETs," in *IEEE MTT-S Int. Microwave Symp. Dig.*, San Francisco, CA, May–June 1984, pp. 267–269.
[36] R. Poore, "Accurate simulation of mixer noise and oscillator phase noise in large RFICs," in *Asia–Pacific Microwave Conf.*, Hong Kong, Dec. 1997, pp. 357–360.
[37] M. C. Sanchez, E. Martin, and J. M. Zamarro, "New vectorial automatic technique for characterization of resonators," *Proc. IEEE*, pt. H, vol. 136, pp. 147–150, Apr. 1989.
[38] A. P. S. Khanna, "Q measurement of microstrip-coupled dielectric resonators," *Microwaves RF*, pp. 81–86, Jan. 1984.
[39] D. Kajfez and J. Guo, "Precision measurement of coupling between TE_{01} mode microstrip and dielectric resonator," *Electron. Lett.*, vol. 30, no. 21, pp. 1771–1772, Oct. 1994.
[40] J. C. Brice, *Properties of Gallium Arsenide*, 2nd ed, ser. EMIS Datareviews 2. London, U.K.: INSPEC/IEE, 1990, pp. 18–19.
[41] T. Lu, G. H. Glover, and K. S. Champlin, "Microwave permittivity of the GaAs lattice at temperatures between 100K and 600K," *Appl. Phys. Lett.*, vol. 13, no. 12, p. 404, Dec. 1968.

Ken'ichi Hosoya (M'98) received the B.A. degree in pure and applied science from the University of Tokyo, Tokyo, Japan, in 1991.

In 1991, he joined the NEC Corporation, Ikaraki, Japan, where he was engaged in the development of millimeter-wave HJFETs and their MMICs for 60-GHz-band wireless communication systems. Since 1998, he has been involved in the development of HBT MMICs for 77-GHz-band automotive radar systems and ultra-high-speed HBT ICs for 40-Gb/s optical communication systems.

Mr. Hosoya is a member of the Institute of Electronics, Information and Communication Engineers (IEICE), Japan. He was the recipient of the Microwave Prize presented at the 1999 Asia–Pacific Microwave Conference, Singapore.

Keiichi Ohata (M'86) received the B.E. and M.E. degrees in electronic engineering from Kyoto University, Kyoto, Japan, in 1970 and 1972, respectively.

In 1972, he joined the Central Research Laboratories, NEC Corporation, Kawasaki, Japan, where he was engaged in the research of ohmic contacts to GaAs, development of low-noise GaAs MESFETs, and research and development of microwave and millimeter-wave heterojunction devices. From 1991 to 1996, he was temporarily transferred to the Advanced Millimeter Wave Technologies Company Ltd., Shiga, Japan, where he was responsible for the research of 60-GHz-band MMICs for short-range communication systems. He is currently a Principal Researcher with the Photonic and Wireless Devices Research Laboratories, NEC Corporation, Otsu, Shiga, Japan, where he is involved with research and development of millimeter-wave devices and transceivers for multimedia communications.

Mr. Ohata is a member of the IEEE Microwave Theory and Techniques Society (IEEE MTT-S), the IEEE Electron Devices Society, and the Institute of Electronics, Information and Communication Engineers (IEICE), Japan.

Takashi Inoue was born in Shiga, Japan, on April 2, 1960. He received the B.S. degree in synthetic chemistry, B.E. degree in applied mathematics and physics, and M.E. degree in molecular engineering from Kyoto University, Kyoto, Japan, in 1983, 1985, and 1987, respectively.

In 1987, he joined the NEC Corporation, Otsu, Shiga, Japan, where he has been engaged in the research and development of the design, fabrication process, and evaluation of integrated circuits. His current interests include the research of compound semiconductor devices for use in microwave and millimeter-wave applications. He is currently a Principal Researcher with the Photonic and Wireless Devices Research Laboratories.

Mr. Inoue is a member of the Institute of Electronics, Information and Communication Engineers (IEICE), Japan.

Masahiro Funabashi received the B.S. degree in electrical engineering from Saitama University, Saitama, Japan, in 1980.

He then joined the NEC Corporation, Kawasaki, Japan, where he has been engaged in the development of microwave integrated circuits. From July 1991 to March 1996, he was with Advanced Millimeter-Wave Technologies. He is currently a Project Manager with the System ULSI Development Division, NEC Corporation.

Masaaki Kuzuhara (M'82–SM'01) received the B.E., M.E., and Ph.D. degrees in electrical engineering from Kyoto University, Kyoto, Japan, in 1979, 1981, and 1991, respectively.

In 1981, he joined the Central Research Laboratories, NEC Corporation, where he has been engaged in research and development on III–V compound semiconductor devices and their integrated circuits. From 1987 to 1988, he was a Visiting Researcher with the University of Illinois at Urbana-Champaign, where he was engaged in modeling and simulation of high-speed III–V heterojunction devices using the Monte Carlo approach. He is currently a Manager with the Photonic and Wireless Devices Research Laboratories, NEC Corporation, Otsu, Shiga, Japan.

Dr. Kuzuhara was the recipient of the 2002 Ichimura Prize presented by the New Technology Development Foundation.